

The Central Velocity Field in NGC 253 : Possible Indication of a Bar

Mousumi Das^{1,2}, K.R. Anantharamaiah^{2,3} & M.S. Yun³

¹Indian Institute of Astrophysics, Koramangala, Bangalore 560 034, India

²Raman Research Institute, C.V Raman Avenue, Sadashivanagar, Bangalore 560 080, India

³National Radio Astronomy Observatory, Socorro, NM 87801, USA

e-mail: mousumi@astro.umd.edu, anantha@rri.ernet.in, myun@daisy.astro.umass.edu

Received _____; accepted _____

ABSTRACT

We have investigated whether motion of gas in a bar-like potential can account for the peculiar but systematic velocity field observed in the nuclear region of the starburst galaxy NGC 253. This unusual velocity field with gradients along both major and minor axes was revealed in a high resolution ($1.8'' \times 1.0''$) H92 α recombination line observation by Anantharamiah and Goss (1996). A simple logarithmic potential is used to model the bar. Assuming that the bulk of the gas flows along closed and non-intersecting x_1 (bar) and x_2 (anti-bar) orbits of the bar potential, we have computed the expected velocity field and position-velocity diagrams and compared them with the observations.

A comparison of the integrated CO intensity maps with the spatial distribution of the x_1 and x_2 orbits in the model indicates that the nuclear molecular gas in NGC 253 lies mainly on the x_2 orbits. We also find that the velocity field observed in the central 100 pc region in the H92 α recombination line is well accounted for by the bar model if most of the ionized gas resides in the inner x_2 orbits. However, the model is unable to explain the velocity field on a larger scale of ~ 500 pc observed using the OVRO interferometer with a resolution of $5'' \times 3''$. The direction of the observed CO velocity field appears twisted compared to the model. We suggest that this perturbation in the velocity field may be due to an accretion event that could have occurred 10^7 years ago.

1. INTRODUCTION

NGC 253 is a nearby, barred Sc galaxy with a nuclear starburst region ($L \sim 3 \times 10^{10} L_{\odot}$; Telesco & Harper 1980). The galaxy has been extensively studied at different wavelengths. The proximity of the galaxy ($d \sim 3.4$ Mpc) and the ongoing nuclear starburst makes it an ideal candidate to study enhanced star formation at nearby distances. The galaxy is nearly edge on ($i = 78^{\circ}$) with a considerable amount of dust in the center which makes it bright in the infrared wave bands. Observations of the $H\alpha$ emission line indicate possible nuclear outflows and stellar winds in the central region, arising from enhanced star formation (Ulrich 1978, Schulz & Wegner 1992). Radio continuum observations reveal numerous compact sources within the inner 200 pc which are either supernova remnants or HII regions (Ulvestad & Antonucci, 1997). At near-infrared wavelengths (NIR), a prominent bar can be observed in the center (Scoville et al. 1985) whose position angle is tilted by about 18° with respect to the major axis of the galaxy. Interferometric CO observations with a resolution of $\sim 5''$ have shown the presence of a molecular bar of dimensions $30'' \times 10''$, whose orientation is similar to the NIR bar (Canzian, Mundy & Scoville, 1988). HCN and CS emissions, which trace dense gas, also reveal a similar bar (Paglione et al 1995 and Peng et al. 1996). Recent work on the bar of NGC 253 indicate that there is at least one Inner Lindblad Resonance (ILR) point for the galaxy (Arnaboldi et al. 1995). Various types of data on NGC 253 indicate that the nuclear starburst is mainly located within a circumnuclear ring in the bar (e.g. Engelbracht et al. 1998).

The kinematics of gas in the nuclear region of NGC 253 has been known to be anomalous from the early $H\alpha$ observations by Demoulin & Burbidge (1970). Radial velocity measurements at various position angles near the nucleus show that, in addition to solid body rotation, large non-circular motions exist within the central region (Ulrich 1978, Schulz & Wigner 1992, Munoz-Tunon, Vilchez & Castaneda 1993). However, due to problems of

obscuration at optical wavelengths, results from $H\alpha$ and $[NII]$ observations are difficult to interpret. Longer wavelength observations such as that of CO (Canzian, Mundy & Scoville 1988), $Br\gamma$ (Puxley and Brand 1995) and H_2 (Prada et al. 1996) indicate steeper velocity gradients along the major axis and only solid body rotation in the central region. Most of the optical and IR observations, aimed at studying the kinematics of the nuclear region of NGC 253 (e.g. Arnaboldi et al. 1995, Prada et al. 1996, Prada, Gutierrez & McKeith 1998, Engelbracht et al. 1998), have relied on measuring the velocity gradients along chosen position angles passing through the nucleus (e.g. major axis and minor axis). However interferometric radio observations at millimeter and centimeter wavelength (e.g. Canzian et al. 1988, Paglione et al. 1995, Anantharamaiah & Goss 1996, Peng et al. 1996) measure two-dimensional velocity fields which provide a more complete picture of the kinematics in the nuclear region. These two-dimensional measurements reveal a complex but systematic velocity pattern in the central region. In addition to solid body rotation, the observed velocity fields indicate motions which may be due to a bar-like potential in the center (Peng et al 1996) or a kinematic sub-system which may be caused by a past merger event (Anantharamaiah & Goss 1996).

The highest resolution measurement of the two-dimensional velocity field available to date is that of Anantharamaiah & Goss (1996) who observed the $H92\alpha$ recombination line with a beam of $1.8'' \times 1.0''$ and a velocity resolution of 54 km s^{-1} . The line emission is detected in the central $9'' \times 4''$ (approximately $150 \text{ pc} \times 60 \text{ pc}$) region of NGC 253 and oriented roughly along the major axis of the galaxy. The observed velocity field of the $H92\alpha$ line emission shown in Figure 1a, has an elongated S-shaped pattern with iso-velocity contours running almost parallel to the major-axis of the galaxy. For pure solid body rotation, the iso-velocity contours are expected to run parallel to the minor-axis. Anantharamaiah & Goss (1996) showed that this velocity field could be fitted to a set of three orthogonally rotating nested rings of ionized gas. Such an interpretation is however

only empirical and has no clear physical basis. The central velocity field of NGC 253 has been observed over a larger scale ($\sim 30'' \times 10''$) but with coarser angular resolution ($\sim 3'' - 6''$) in molecular lines; CO (Canzian et al. 1988), HCN (Paglione et al. 1995) and CS (Peng et al 1996). As mentioned earlier the molecular line emission is oriented along the NIR bar which is tilted by 18° with respect to the major axis whereas the H92 α line emission is mainly along the major axis. The velocity field of the molecular gas is also distinctly different from that of the ionized gas. Peng et al. (1996) have suggested that the morphology and kinematics of the dense molecular gas can be explained by gas moving in a bar potential.

In this paper, we have attempted to model the inner velocity field of NGC 253 to determine whether the velocity pattern observed by Anantharamaiah & Goss (1996) can also be explained by motion of gas in a bar potential. We also present in this paper, new observations of the velocity field in the CO line with an angular resolution of $5.6'' \times 2.6''$. Since gas is a collisional system (unlike stars which can be collisionless), it tends to settle on closed, non-intersecting orbits in the bar potential. Using a bar model, we have determined a set of closed orbits from which a velocity field is derived and compared with observation in the H92 α and the CO lines. While the bar model successfully accounts for the velocity field observed in the H92 α line in the inner ($9'' \times 4''$) region, it does not account of the observed CO velocities on a larger scale ($40'' \times 15''$). The only earlier attempt to model the nuclear velocity field of NGC 253 using a bar model is that of Peng et al (1996) who attempted to explain the velocity field observed on the larger scale in the CS line. Although, Peng et al (1996) have reported success of their model, by comparing observed position-velocity (PV) diagrams with PV plots of closed x1 and x2 orbits, we show in this paper that a single bar model cannot explain both the H92 α and the CO (or the CS) velocity fields.

2. New Observations of the CO Velocity field

In Figure 1b, we show a new measurement of the velocity field of ^{12}CO obtained using the Owens Valley Radio Interferometer. The angular resolution is $5.6'' \times 2.6''$. These observations were made as a part of a detailed study of molecular gas in the nuclear region of NGC 253, which will be published elsewhere (Yun et al., in preparation). A comparison of Figs 1a and 1b shows that there are several differences in the velocity fields observed in the $\text{H}92\alpha$ and the CO lines. While the CO emission occurs over a much larger region ($\sim 40'' \times 15''$), the $\text{H}92\alpha$ line is confined to the inner most region ($\sim 9'' \times 4''$). The position angles of the two emission regions are different: while the $\text{H}92\alpha$ line emission is along the major axis of the galaxy ($\text{PA} = 52^\circ$), the CO emission is oriented along the axis of the NIR bar ($\text{PA} = 70^\circ$). The iso-velocity contours in Figures 1a and 1b run along entirely different position angles. Some distortion in the CO velocity field is seen at the position where the $\text{H}92\alpha$ emission is observed. It is possible that, at higher angular resolution, the CO velocity field may resemble the $\text{H}92\alpha$ velocity field in the central region. The iso-velocity contours in Figure 1b also do not run parallel to the minor axis of the galaxy indicating that the kinematics of the CO gas is not dominated by standard galactic rotation. The velocity field observed by Peng et al. (1996) in the CS line is similar, but less systematic compared to the CO velocity field in Figure 1b.

3. Motion of Gas in the Bar Potential

Gas clouds dissipate energy through collisions. Hence such clouds will tend to move along closed orbits in a plane. In a bar potential, there are two types of closed orbits in the plane of the galaxy; the x_1 (bar) orbits which are extended along the major axis of the bar and the x_2 (anti-bar) orbits which are oriented perpendicular to the major axis of the bar (Contopoulos & Mertzanides, 1977, Athanassoula, 1988, Binney & Tremaine, 1987).

The x_2 orbits exist if there is an Inner Lindblad Resonance (ILR) ring in the galaxy, which occur at radii where the relation $\Omega(R) - \Omega_b = \kappa(R)/2$ is satisfied. Here $\Omega(R)$ is the angular speed of the particle, Ω_b is the angular speed of the bar and κ is the epicyclic frequency. Physically, this means that a particle rotating in the bar potential with angular speed $\Omega(R)$, will encounter successive crests of the bar potential at a frequency equal to half its epicyclic frequency. For radii close to the ILR radius, a particle leads the bar and for radii near the Outer Lindblad Resonance (OLR), the particle lags behind the bar. At radii where $\Omega(R) - \Omega_b = 0$, a particle is stationary in the rotating potential. More than one ILR can exist; in fact from the optical rotation curve of NGC 253, Arnaboldi et al. (1995) conclude that there are two ILRs in the bar of NGC 253, one at a radius of $25''$ and the other close to the center.

At the intersection of the x_1 and x_2 orbits, gas clouds may collide, lose angular momentum and sink into the x_2 orbits. Simulations of gas evolution in bars have shown that an evolved bar has relatively more gas on the inner orbits than on the outer orbits (Friedli & Benz, 1993). Within the bar of NGC 253, there is a $\sim 20''$ diameter nuclear ring of dense star forming gas (Arnaboldi et al 1995) which may imply that there is a significant amount of gas on x_2 orbits within the bar. We therefore use the x_1 and x_2 orbits to model the gas flow in the center of NGC 253. This method of explaining gas kinematics in a bar potential was first introduced by Binney et al. (1991) for the distribution of gas in the Galactic Center. Since then, this method has been applied to many barred galaxies (e.g. Achtermann & Lacy, 1995). This approach was used by Peng et al. (1996) to explain the distribution of dense gas in the bar of NGC 253. Peng et al. (1996) plotted the position velocity (P-V) diagram for closed orbits in the bar model and compared it with the observed P-V diagram for the CS line emission. Based on this comparison, they interpreted the regions of CS emission as the apocenters in the x_1 and x_2 orbits of the bar potential.

An alternative approach to determine the velocity field is the technique of hydrodynamic simulation of gas flow in a bar potential (e.g. Piner, Stone and Teuben, 1995, Athanassoula, 1992). In hydro simulations it is possible to follow the evolution of the gas in the bar and to trace the formation of shocks in the gas. However, the closed orbits method which is used in this paper, gives an explicit picture of the distribution of the gas. The distribution of the orbits shows the regions where gas can settle (the orbits themselves) and the regions where gas will pile up in shocks (i.e. at the ends of the bar and the crossing points of the x_1 and x_2 orbits). In this method, the velocity field can also be explicitly obtained and compared with the observations.

Although we also adopt a bar model and the closed-orbits method, which is similar to that of Peng et al. (1996), our approach differs in at least two ways. First, in constructing the bar model, Peng et al. (1996) used a logarithmic bar potential and scaled all length scales with the disk rotation velocity v_b . When comparing the closed orbits with the observed distribution of CS intensity and the P-V plot, Peng et al. (1996) scaled the orbits with $v_b = 75 \text{ kms}^{-1}$. However, the velocity in the flat portion of the rotation curve is $\approx 200 \text{ kms}^{-1}$ (Arnaboldi et al. 1995). The value $v_b = 75 \text{ kms}^{-1}$ leads to a bar structure in which the x_1 orbits extend out to $\sim 20''$ resulting in a bar size of $\leq 45''$. However, IR and optical observations estimate a bar size of $\sim 150''$ (e.g. Scoville et al. 1985). Our bar model incorporates parameters from the rotation curve and hence leads to a more realistic bar size. In the bar model presented in the following sections, we have used $v_b = 200 \text{ kms}^{-1}$. This velocity gives a bar size of $\approx 200''$, which is closer to the observed value than that used by Peng et al. (1996). The large size of the bar may indicate that not all of the outer x_1 orbits support gas and hence star formation; most of the gas might have been funnelled into the inner orbits.

The second difference between the work presented here and that of Peng et al (1996)

is that, in addition to comparing the model and observed P-V diagrams, we construct a model two-dimensional velocity field and compare it with the observed velocity fields shown in Figs 1a and 1b. We show that an explicit comparison of the predicted and model velocity fields is indeed essential to determine whether the gas is actually moving on regular x_1 and x_2 orbits. Because of the inherent degeneracy in projection, a wide range of models can fit the P-V plot, whereas the added dimension in the 2-D velocity field helps differentiating the models.

3.1. Bar Potential and Parameters

For simplicity we have also adopted a logarithmic bar potential to model the velocity field. The potential is given by,

$$\Phi(x, y) = \frac{1}{2}(v_b)^2 \ln(x^2 + \frac{y^2}{q^2} + R_c^2) \quad (1)$$

(Binney & Tremaine, 1987), where v_b is the velocity in the flat portion of the rotation curve of the galaxy, q is the non-axisymmetry parameter and R_c is the core radius. If the bar is rotating with an angular velocity Ω_b , then the equation of motion of a particle moving in the rotating frame of the bar is given by

$$\ddot{\mathbf{r}} = -\nabla\Phi - 2(\boldsymbol{\Omega}_b \times \mathbf{v}) - \boldsymbol{\Omega}_b \times (\boldsymbol{\Omega}_b \times \mathbf{r}), \quad (2)$$

where \mathbf{r} is the position vector of a particle in the bar, \mathbf{v} is the velocity of a particle in the rotating frame of the bar and $\ddot{\mathbf{r}}$ is the acceleration.

The closed orbits in the bar potential were determined for different values of q and R_c . Some of the outer x_1 orbits which are elongated along the length of the bar, are looped i.e. self intersecting at the ends. Since gas clouds cannot survive in these orbits due to collisions at the intersection points, these orbits were excluded while determining the velocity field.

The free parameters were chosen such that the number of looped orbits is minimum. The parameters defining the bar potential are v_b , Ω_b , q and R_c . Of these four parameters, v_b and Ω_b can be determined from the rotation curve. These parameters were taken from the optical rotation curve observed by Arnaboldi et al. (1995). The velocity in the flat portion of their rotation curve is $v_b \sim 200 \text{ kms}^{-1}$ and the angular rotation velocity of the bar is $\Omega_b = 48 \text{ kms}^{-1}\text{kpc}^{-1}$. The adapted parameters of the galaxy are given in Table 1.

Closed orbits were determined for values of the the non-axisymmetry parameter q in the range 0.7 to 0.9. For lower values of q , most of the closed orbits are looped. Even for $q=0.7$, most of the outer x_1 orbits are looped at the ends. For $q=0.9$, the bar structure is not as pronounced as that for the $q=0.7$ & 0.8 models but the non-axisymmetry is clearly seen. For both $q = 0.8$ and 0.9, we obtain a large range of non-looped x_1 and x_2 orbits. The models presented in this paper are for $q=0.8$ & 0.9. For both values of the parameter, there is a region of overlapping x_1 and x_2 orbits. At these points the clouds collide, lose angular momentum and sink into the center. This process is thought to be important for transporting gas into the center of the galaxy (Binney et al. 1991, Friedli & Benz 1993).

The other free parameter in the bar model, core radius R_c , was varied from 0.05 pc to a few hundred parsecs. For R_c less than a few parsecs, the velocity field resembles that of a simple flat rotation curve, i.e. it appears like the ‘spider diagram’ observed in the disks of galaxies. For $R_c > 200$ pc, distinct x_1 and x_2 orbits are not obtained. The range $5 \text{ pc} \ll R_c < 200 \text{ pc}$ gives a bar structure and a velocity field which is different from that expected from normal galactic rotation. We examined the velocity fields for values of core radii $R_c = 50 \text{ pc}$, 100 pc and 150 pc and found them to be similar. In the following sections, results are presented for $R_c=100 \text{ pc}$.

3.2. Bar and Anti-Bar Orbits

Figures 2a & 2b show the closed orbits in the bar potential in the plane of the galaxy as they appear when the galaxy is viewed face on. For these orbits, the non-axisymmetry parameter $q=0.8$ and 0.9 respectively and the core radius $R_c = 100$ pc. The closed orbits were also determined for the same value of q and $R_c = 50$ pc and 150 pc. The overall appearance of the bar is the same for all the three cases. The extent of the x_1 orbits is approximately 3.2 kpc ($3'.2$) in all the cases and their orientation is also similar. Since gas will settle along non-looped x_1 and x_2 orbits in the bar potential, the radial extent of the bar in this model is 3.2 kpc. This radial extent is comparable to the size of the NIR bar observed by Scoville et al. (1985). The inner x_2 orbits extend out to about 400 pc ($\sim 25''$) along the semi-major axis. The x_2 orbits corresponding to different core radii do differ from one another. For core radii 100 pc and 150 pc, the x_2 orbits within 20 pc are aligned perpendicular to the other x_2 orbits i.e. along the x_1 orbits. The result is a bar within a bar structure. However, if the orbits are convolved with a two dimensional Gaussian representing the telescope beam, these innermost perpendicular orbits, which are lying within the x_2 orbits, are no longer distinct. Thus in the final convolved velocity fields, there are no significant differences between models with core radii lying in the range 5 pc $\ll R_c < 200$ pc.

In order to compare the model velocity field with the observations, the closed orbits were projected on to the plane of the sky. Projections were made using the parameters given in Table 1. If the bar orbits are projected on the plane of the sky, the size and orientation of the x_1 and x_2 orbits change significantly as shown in Figures 3a & 3b. The x_1 orbits are aligned along the bar (PA = 70°). The x_2 orbits do not appear to be perpendicular to the x_1 orbits. Instead, these orbits are at a position angle of 45° on the plane of the sky which is 7° with respect to the major axis of the galaxy. This inner ring appears like a narrow

ridge when projected on the plane of the sky even though it has a radius of ~ 350 pc. In the plane of the sky, the inner ring is also nearly aligned with the major axis of the galaxy rather than the axis of the bar. This alignment is due to the projection of the x_2 orbits on the sky and has been discussed by others (e.g. Böker, Krabbe & Storey, 1998). This inner ring can be identified with the ring of star forming regions and supernova remnants which have been observed both in the optical and radio bands (Arnaboldi et al. 1995, Baan et al. 1997). A large number of compact radio sources have been observed in the inner 200 pc of NGC 253 which are identified as supernova remnants and HII regions (Ulvestad & Antonucci 1997). A high concentration of dense molecular gas is also observed in the inner ring within the bar (e.g. Peng et al. 1996).

A comparison of the extent of the projected bar orbits in Fig 3, with the observed extents of CO, CS and HCN emissions, shows that the molecular gas must lie mainly on the x_2 orbits. The molecular gas lies within a radius of $30''$ from the center, within which, only one (the inner most) x_1 orbit is present (Fig 3). Within the region of molecular emission, the computed orbits are mainly of the x_2 -type for both $q=0.8$ and 0.9 . All the molecular line observations thus indicate that gas has been channelled in to the inner most orbits inside the bar and the resulting high concentration of gas may have given rise to a burst of nuclear star formation. We note that in the bar model considered by Peng et al (1996), the molecular gas is present in the outer x_1 orbits as well. This difference is because, Peng et al (1996) have implicitly assumed a smaller size for the bar.

4. Comparison with Observations

4.1. The Velocity Field

To obtain the velocity field expected in the bar model and compare it to the observations, the radial velocity at each point along the closed orbits was determined by transforming the velocity components in the rotating frame of the bar to the inertial frame using

$$\mathbf{v}_{\text{in}} = \mathbf{v}(\mathbf{x}, \mathbf{y}) + \boldsymbol{\Omega}_{\text{b}} \times \mathbf{r}. \quad (3)$$

The radial velocity is given by

$$\mathbf{v}_{\text{rad}} = [(v_x - \Omega_b y) \sin \phi + (v_y + \Omega_b x) \cos \phi] \sin(i). \quad (4)$$

Hence, for every point $\mathbf{r}(\mathbf{x}, \mathbf{y})$ along the closed orbit, there is a corresponding radial velocity \mathbf{v}_{rad} . Using the above equation, it is possible to plot isovelocity contours for the radial velocities of the closed bar orbits projected onto the plane of the sky. To make a proper comparison with the observations, the model velocity field is convolved with an appropriate two dimensional Gaussian representing the telescope beam. The comparison between model and observed velocity fields has the limitation that while the observed velocity field is "weighted" by the intensity of line emission, the model velocity field is based only on the distribution of closed orbits. In other words, the model implicitly assumes that the gas is uniformly distributed over all the closed orbits.

Figure 4a shows the model velocity field within the inner $8''$ derived from the closed orbits shown in Figure 2a ($q=0.8$). Figure 5a is the corresponding velocity field for the orbits shown in Figure 2b ($q=0.9$). The convolving Gaussian function has a size $1.8'' \times 1''$ which is similar to the resolution used by Anantharamaiah & Goss (1996) in their H92 α observations. A comparison of Fig 1a with Fig 3 reveals a remarkable correspondence between the observed and model velocity fields in the central region for both q values. The model velocity field predicts isovelocity contours which are nearly parallel to the major axis as observed. The S-shaped pattern in the observed field is also present to some extent in

the model velocity field. It thus appears that most of the ionized gas observed in the H92 α line by Anantharamaiah & Goss (1996) can be associated with the x_2 orbits of the bar potential.

The velocity gradients along the major and minor axes of the galaxy in the inner region of the model can be quantitatively compared with the values obtained by Anantharamaiah & Goss (1996) . For $q=0.8$ and $R_c = 50$ pc to 150 pc, the bar model predicts a velocity gradient along the minor axis of ~ 25 to 30 $\text{kms}^{-1}\text{arcsec}^{-1}$ and the gradient along the major axis is ~ 10 to 15 $\text{kms}^{-1}\text{arcsec}^{-1}$. Anantharamaiah & Goss (1996) measured a gradient of ~ 18 $\text{kms}^{-1}\text{arcsec}^{-1}$ along the minor axis and ~ 11 $\text{kms}^{-1}\text{arcsec}^{-1}$ along the major axis of the galaxy. The estimates from the model are thus comparable to the observed values.

Figure 4b shows the model velocity field for the parameter $q=0.8$, on a larger scale of $54'' \times 30''$ and Figure 5b is the corresponding velocity field for $q=0.9$. These figures should be compared with the CO velocity field shown in Figure 1b. The angular resolution is $5'' \times 3''$. The region covered in the figures includes mainly all of the x_2 orbits. The model velocity field appears somewhat different for the two q values. The $q=0.9$ contours have a closer resemblance to the observed velocity field (Figure 1b) than the $q=0.8$ model. The velocity field lines for $q=0.9$ are more spread out than the $q=0.8$ model and beyond $5''$ have a downward slope which matches fairly well with the observed field. To see if the velocity field in Figure 1b could be reproduced by including only a subset of the orbits, we first constructed the velocity field with just the x_2 orbits and then with the x_2 and a few of the inner x_1 orbits. In both cases, we were not able to construct a velocity field similar to that observed in CO and other molecular lines.

We thus come to the conclusion that the model of the bar potential can only explain the velocity field close to the nucleus and not on the scale of $45''$ shown in Figure 1b. We conjecture that there is some perturbation within the bar which causes a change in

the direction of the bar at progressively larger radii. Such a change in the position angle of the bar with radial distance has in fact been observed by Baan et al (1997) in the formaldehyde absorption line. They conclude that there must be a warped gas disk in the nuclear region which results in the changing direction of the bar with radius. However, the gross appearance of the bar does not seem to be affected by the perturbed velocity field. In Section 4 we consider a possible scenario to explain the difference between the observed and model CO velocity fields. Our conclusion, based on a comparison of the velocity field is thus different from that of Peng et al (1996) who compared the PV diagrams and concluded that the bar model can account for the velocities observed on a larger scale in molecular lines. In the next section we carry out such a comparison of the PV diagrams.

4.2. Position-Velocity Diagram

The closed orbits in a bar potential can also be used to construct a P-V diagram and has been done for NGC 253 and a few other galaxies in the literature (e.g. Peng et al. 1996, Achtermann & Lacy 1995). But the resultant P-V plot has two major differences with the observed P-V diagram. First, in the model P-V plot, V is just the rotational velocity of the gas in the bar potential (V_0); the velocity spread Δv is not incorporated in the model. If the gas is cold, like molecular hydrogen, then Δv may be relatively small and this difference may not be important. But if the gas is hot and turbulent, then Δv may be fairly large. Secondly, the model P-V plot does not include information about the intensity (I) of the line emission from the gas. The second problem can be partially overcome by assuming that the intensity is proportional to the gas distribution in the bar. Thus if the gas is uniformly distributed over the closed orbits, then the intensity is proportional to the number of orbits crossing through that region. We gridded the P-V plane so that each grid point had a set of coordinates (P,V,I). The size of the grid unit was chosen to be much smaller than the

beam of the telescope. For example, in the inner $9''$ of NGC 253, we used a grid unit size of $0.3'' \times 8 \text{ kms}^{-1}$. The “beam” used to observe that region is $1.6'' \times 54 \text{ kms}^{-1}$ (Anantharamaiah & Goss (1996)). This grid or 2-d matrix was then convolved with a 2-d Gaussian matrix representing the beam of the telescope.

Figure 6a is the P-V diagram of the nuclear ionized gas in NGC 253 observed in the $\text{H}92\alpha$ radio recombination line by Anantharamaiah & Goss (1996) . There is a large velocity spread in the center of about 400 kms^{-1} and two secondary peaks are seen on either side of the central peak. A velocity gradient ($\sim 10 \text{ kms}^{-1}$) is clearly seen. Figure 6b is the beam-convolved model P-V diagram of the inner $8''$ constructed from the x_1 and x_2 orbits, as discussed above. Considering the simplicity of our model, there is a reasonable agreement between the two plots. Although the intensity contours in the model are in arbitrary units, there is an overall similarity which includes the presence of a main peak and two secondary peaks, although the latter are not as pronounced as in the observed P-V plot. Furthermore, the velocity gradient is in the right sense. The velocity spread near the central peak and the magnitude of the velocity gradient are, however, less than the observed values in Figure 6a. Some of the differences may be caused by the fact that the observed P-V plot is constructed from the $\text{H}92\alpha$ radio recombination line which is emitted from hot, possibly turbulent, ionized gas for which the velocity spread could be quite large. This velocity spread is not included in the model.

Figure 7a shows a P-V diagram along the major axis observed on a much larger scale ($\sim 45''$) in CO, using the OVRO synthesis array (Sec 2). There are two strong peaks on either side of the center and a gradient in velocity from NE to SW. Figure 7b shows the beam-convolved model P-V diagram over a similar region for $q=0.8$. The P-V plots for $q=0.8$ & 0.9 are very similar and so we have shown only the $q=0.8$ figure in the paper. There is a reasonable similarity between the model and observed P-V plots. The extent

and gradient of the velocity field shown in Figure 7b agrees fairly well with that in Figure 7a. On the basis of this plot, we could conclude that the model explains the observed kinematics of molecular gas. Such a conclusion was in fact arrived at by Peng et al. (1996) who compared their observed P-V diagram (in the CS line) with the x_1 and x_2 orbits projected on to the P-V plane. There is also a similarity between the model P-V plots in Fig 7b and that observed in the CS line by Peng et al. (1996). However, as shown in the previous section, there is no similarity between the observed CO velocity field (Figure 1b) and the model velocity field (Figures 4b & 5b). We, therefore, conclude that the velocity field observed on larger scales in molecular gas (Canzian et al. 1988, Peng et al. 1996 and Figure 1b) is not explained by the bar potential, although the observed and model P-V diagrams have many similarities. Thus an agreement between the observed and expected P-V diagram is a necessary but not sufficient condition to ascertain whether a particular model accounts for the observed velocity field. It is necessary to also compare the 2-d velocity field predicted by the model with the observations.

A careful comparison of the larger scale (~ 500 pc) observed and model velocity fields (Figures 1b and 7b) shows that it may be possible to interpret the observed field as a twisted version of the model field. It is possible that the velocity field can indeed be due to the bar potential, but an additional perturbation has altered the velocity structure. In the next section we conjecture that this perturbation was caused by an accretion event that occurred in the recent past.

5. Does the Velocity Field Reveal Evidence of a Merger ?

NGC 253 is considered to be a strong, nuclear starburst galaxy with star formation concentrated within the inner x_2 ring of the bar (Peng et al. 1996). Though a bar can produce enhanced star formation in the center of a galaxy, the rapid fueling of gas in a

bar can also be triggered by the accretion of a small satellite galaxy (Mihos & Hernquist, 1994). That such an accretion event may have occurred in NGC 253 has been suggested by Anantharamaiah & Goss (1996) and Prada, Gutierrez & McKeith (1998).

In the previous section, we showed that the nuclear velocity field can be explained reasonably well by gas moving on x_2 orbits within the bar. But as we move out to radii of $\sim 30''$ and farther, we find that there is no agreement with the observations. This disagreement is possibly due to the change in the position angle of the bar which has been observed on scales of ~ 1 kpc (Baan et al. 1997). Such a perturbation of the bar potential could have been caused by the postulated merger event in the recent history of the galaxy. However, since the velocity field at large distances from the starburst region is regular and the outer HI contours are also regular (Combes 1977, Puche 1991), the merger event has not caused any disruption on a large scale. Therefore, if there was a merger in the recent past, then the accreted mass must be fairly small compared to the mass of the galaxy.

The perturbation in the velocity field is observed at radii of $\sim 30''$ and larger, which corresponds to gas moving on the outer x_2 orbits in the bar. The gas in the inner ~ 100 pc, which is moving along inner x_2 orbits, does not seem to have been perturbed since the observed velocity field is similar to that predicted by the model. This behavior may be explained by the difference in the rotation velocities for gas moving along the outer and inner x_2 orbits. The rotation time scales for gas moving in the inner (< 100 pc) orbits in our model is \sim few times 10^6 years while that for the outer x_2 orbits is \sim few times 10^7 years. Thus the model suggests that the very inner gas is moving at least ten times faster than the gas in the outer x_2 orbits. Perturbations in the central potential due to the accretion of a small galaxy may have been smoothed out by the faster rotating inner gas but its effect may still remain on the scale of the outer x_2 orbits where gas is rotating more slowly. The accretion event may thus have occurred about 10^7 years ago.

We have used the above hypothesis to determine an approximate mass for the accreted galaxy using the theory of dynamical friction. From Binney & Tremaine (1987), the deceleration of a body of mass M moving through a region of mass density ρ , is given by,

$$\frac{dv_M}{dt} = \frac{4\pi(\ln\Lambda)G^2\rho M}{v_M^2} \left[\text{erf}(X) - \frac{2Xe^{-X}}{\sqrt{\pi}} \right] \quad (5)$$

where $X = \frac{v}{\sqrt{2}\sigma} \sim 1$ and $\ln\Lambda \sim 10$ to 20 (see Binney & Tremaine, 1987, pg 429). The density ρ can be determined from the dynamical mass within the inner $5''$ (~ 150 pc), which is $\sim 3 \times 10^8 M_\odot$ (Anantharamaiah & Goss, 1996). The accreted mass is then given by,

$$M = \frac{v_M^3}{12\pi(\ln\Lambda)G^2\rho \left[\text{erf}(X) - \frac{2Xe^{-X}}{\sqrt{\pi}} \right] \Delta t} \quad (6)$$

If we assume that Δt is the time taken for the mass M to sink through the inner 300 pc, then $\Delta t \sim 10^7$ years. This time scale is similar to the time required for the perturbation to have been smoothed out in the inner x_2 orbital region but the perturbation may still be persisting in the outer x_2 orbital region. We have taken v_M to be the rotation speed at 300 pc which is $\sim 110 \text{ km s}^{-1}$ (Arnaboldi et al. 1996). Using these values, the mass of the accreted body $M \sim 10^6 M_\odot$. This mass is too small to represent a galaxy but it may represent the remains of an accreted galaxy which had most of its outer gas and stars stripped off during the infall. In deep optical images of NGC 253, made using image enhancement techniques (Malin 1981; Beck, Hutschenreiter and Wielebinski 1982), a distortion in the disk is observed with a spur of emission protruding to the south. It is possible that this distortion is an imprint left by the merger event that occurred 10^7 years ago as we have hypothesized above. Also, Watson et al. (1996) have detected four star clusters in the inner parsecs of NGC 253, one of which, has a mass of $\sim 1.5 \times 10^6 M_\odot$ and the others have masses of the order of $10^4 M_\odot$. The more massive cluster may be the remains of the accreted mass which has perturbed

the bar potential.

6. SUMMARY

We have attempted to model the observed nuclear velocity field of ionized and molecular gas in NGC 253 using a simple logarithmic bar potential. The parameters for the potential were derived from the optical rotation curve. The velocity field was determined from the x_1 and x_2 orbits in the bar potential and compared with observations of the H92 α (Anantharamaiah & Goss 1996) and CO lines. The results are summarized below.

- 1) The x_2 orbits, projected onto the plane of the sky, lie roughly along the major axis of the galaxy. The x_2 ring appears very narrow and ridge like. We identify the ionized gas observed in the H92 α line as lying along the inner x_2 orbits. Also, when we compare the integrated CO intensity maps in the literature with the model we find that the molecular gas is also distributed mainly over the x_2 orbits.
- 2) The velocity field within the inner 8'' predicted from the bar potential is similar to that observed by Anantharamaiah & Goss (1996). The model predicts velocity gradients both along the major and minor axes. The isovelocity contours run parallel to the major axis as observed. The model P-V diagram agrees reasonably well with the observations.
- 3) The model velocity field on a larger scale ($\sim 45''$) is significantly different from the observed velocity fields in CO and CS (Peng et al. 1996). However, the model P-V diagrams agree reasonably with the observations. We therefore conclude that agreement in P-V diagrams is a necessary but not sufficient condition to explain the complete velocity field.
- 4) The observed velocity field on a larger scale ($\sim 45''$) appears to be a twisted version of the model velocity field with the direction of the gradient changing with radius. We suggest that this perturbation may have been caused by the accretion of an object with mass of

$\sim 10^6 M_\odot$ about 10^7 years ago. This accretion event may also have triggered the nuclear starburst observed in the galaxy. Enhanced optical images of NGC 253 (Malin 1981, Beck et al 1982) show a distortion in the outer regions of the galactic disk which may be a signature left by the merger event.

We thank Niruj R. Mohan for useful suggestions regarding the isovelocity contour plots and the P-V diagrams and W.M. Goss for a critical reading of the manuscript. The National Radio Astronomy Observatory is a facility of the National Science Foundation operated under cooperative agreement by Associated Universities, Inc.

FIGURE CAPTIONS

Figure 1 (a) Velocity Field of the central $9''$ observed in the $H92\alpha$ line using the VLA by Anantharamaiah & Goss (1996) , with a resolution of $1.8'' \times 1.0''$. RA and Dec offsets are with respect to the position $(\alpha, \delta) 1950\ 00^h\ 45^m\ 5.80, -25\ 33\ 39.1$. Contour levels range from $70\ \text{kms}^{-1}$ to $270\ \text{kms}^{-1}$ in steps of $10\ \text{kms}^{-1}$. The grey scale ranges from $100\ \text{kms}^{-1}$ to $400\ \text{kms}^{-1}$.

(b) Intensity weighted mean velocity field derived from the CO (1–0) data imaged using the OVRO synthesis array at a resolution of $5''.6 \times 2''.6$ (PA = -2°).

The RA and Dec offsets are with respect to the radio nucleus position $(\alpha(1950) = 00^h 45^m 05^s.79, \delta(1950) = -25^\circ 33' 39''.08)$. Contour levels range from $100\ \text{kms}^{-1}$ to $360\ \text{kms}^{-1}$ in steps of $20\ \text{kms}^{-1}$. The grey scale ranges from $100\ \text{kms}^{-1}$ to $400\ \text{kms}^{-1}$.

Figure 2a. A face-on view of closed orbits in the bar potential in the plane of the galaxy NGC 253. The bar parameters are $v_b=200\ \text{kms}^{-1}$, $\Omega_b=48\ \text{kms}^{-1}\text{kpc}^{-1}$, $q=0.8$, $R_c=100\text{pc}$. The outer x_1 orbits lie along the bar major axis and the inner x_2 orbits lie along the bar minor axis.

Figure 2b. A face-on view of closed orbits in the bar potential for the bar parameters $v_b=200\ \text{kms}^{-1}$, $\Omega_b=48\ \text{kms}^{-1}\text{kpc}^{-1}$, $q=0.9$, $R_c=100\text{pc}$.

Figure 3a. Closed orbits in Figure 2a projected onto the plane of the sky. The galaxy has a position angle of 52° and the PA of the bar is 70° . In this projection, the outer x_1 orbits lie along the bar and the inner x_2 orbits have a position angle of 45° .

Figure 3b. Closed orbits in Figure 2b projected onto the plane of the sky. As in Figure 3a, the galaxy has a position angle of 52° and the PA of the bar is 70° . The outer x_1 orbits lie along the bar and the inner x_2 orbits have a position angle of 45° .

Figure 4a. Model radial velocity field in the central $8''$, constructed from closed orbits in the bar potential of Figure 2a. The model is convolved with a Gaussian beam $1.8'' \times 1.0''$, which is equal to the beam in Figure 1a. Contours are marked in units of kms^{-1} . The radial velocities are offset with respect to the central velocity of the galaxy. The dashed rectangular box shows the region where the $\text{H}92\alpha$ line is observed (see Figure 1a).

Figure 4b. Model radial velocity field in the central $8''$, constructed from closed orbits in the bar potential of Figure 2b. The model is convolved with a Gaussian beam $1.8'' \times 1.0''$. Contour levels are marked in kms^{-1} and as before the radial velocities are offset with respect to the center of the galaxy. The dashed rectangular box shows the region where the $\text{H}92\alpha$ line is observed (see Figure 1a).

Figure 5a. Model radial velocity field in the central $54'' \times 30''$ constructed from the closed orbits in the bar potential of Figure 2a. The model is convolved a with Gaussian function of dimension $5'' \times 3''$ which is the same as the resolution in Figure 1b. Contours are marked in units of kms^{-1} . The radial velocities are offset with respect to the central velocity of the galaxy. The dashed parallelogram shows the region from which the CO line is observed (see Figure 1b).

Figure 5b. Model radial velocity field in the central $54'' \times 30''$ constructed from the closed orbits in the bar potential of Figure 2b. The model is convolved with a Gaussian function of dimension $5'' \times 3''$. Contours are marked in units of kms^{-1} and the velocities are offset from the center of the galaxy. The dashed parallelogram shows the region from which the CO line is observed (see Figure 1b).

Figure 6a. Position velocity diagram of the ionized gas in the inner $8''$ along the major axis of NGC 253. The diagram is constructed from the $\text{H}92\alpha$ recombination line data of Anantharamaiah & Goss (1996) with a spatial resolution of $1.8'' \times 1''$ and a velocity resolution of 54 kms^{-1} . Contour levels are 2, 4, 6, ..., 24 mJy beam^{-1} . Offsets along the Y

axis are from $v_{\text{Hel}} = 200 \text{ km s}^{-1}$. Offsets along the X axis are from $\text{RA}(1950) = 00^{\text{h}} 45^{\text{m}} 5^{\text{s}}.9$.

Figure 6b. Position velocity diagram of the gas moving along the closed orbits in the inner $8''$ constructed from the closed orbits in the bar potential of Figure 2a. The intensity is assumed to be proportional to the orbit number density. The image is convolved with a Gaussian function of size $1.5'' \times 56 \text{ km s}^{-1}$, which is similar to the resolution in Figure 6a. The contour levels are in arbitrary units.

Figure 7a. Position-Velocity plot of the CO (1–0) emission along the morphological major axis of NGC 253 ($PA = 51^\circ$) observed using the OVRO synthesis array. The major axis offset is with respect to the radio nucleus position $(\alpha, \delta) 1950 00^{\text{h}} 45^{\text{m}} 5.80, -25 33 39.1$. and the velocity offset at zero corresponds to the LSR velocity of $+239 \text{ km sec}^{-1}$. The CO line intensity is shown both in greyscale and in contours, which are linear increments of 0.4 Jy beam^{-1} (2σ). The velocity resolution is 20.8 km s^{-1} .

Figure 7b. Model P-V diagram constructed from closed orbits of Figure 2a for the inner $45''$. The intensity is assumed to be proportional to the number density of orbits. The convolving function has size of $6'' \times 20 \text{ km s}^{-1}$, which is similar to the beam resolution in Figure 7a. The contour levels are in arbitrary units.

REFERENCES

- Achtermann, J.M. & Lacy, J.H. 1995, *ApJ*, 439, 163
- Anantharamaiah, K. R. & Goss, W. M. 1996, *ApJ*, 466, L13
- Arnaboldi, M., Capaccioli, M., Capellaro, E., Held, E. V., & Koribalski, B. 1995, *AJ*, 110, 199
- Athanassoula, E. 1988, Proc. of the Joint Varenna-Abastumani International School & Workshop on Plasma Physics, eds T. D. Guyenne & J. J. Hunt (ESA, SP-285, Vol I), 341
- Athanassoula, E. 1992, *MNRAS*, 259, 345
- Baan, W. A., Braag, A. E., Henkel, C., Wilson, T. L. 1997, *ApJ*, 491,
- Beck, R., Hutshenreiter, G. & Wielebinsky, R. 1982, *A&A*. 106, 112
- Binney, J., Tremaine, S. 1987, *Galactic Dynamics* (Princeton Univ. Press)
- Binney, J., Gerhard, O. E., Stark, A. A., Bally, J. & Uchida, K. I. 1991, *MNRAS*, 252, 210
- Böker, T., Krabbe, A. & Storey, J. W. V. 1998, *ApJ*, 498, L115
- Canzian, B., Mundy, L. G., & Scoville, N. Z. 1988, *ApJ* 333, 157
- Combes, F., Gottesman, S.T. & Weliachew, L. 1977, *A&A*, 59, 181
- Contopoulos, G. & Mertzianides, C. 1977, *A&A*, 61, 477
- Engelbracht, C. W., Rieke, M. J., Rieke, G. H., Kelly, D. M., Achtermann, J. M., 1998, *ApJ*, 505, 639
- Forbes, D. A. & Depoy, D. L. 1992, *A&A*, 259, 97
- Friedli, D. & Benz, W. 1993, *A&A*, 268, 65
- Mihos, J.C. & Hernquist, L. 1994, *ApJ*, 425, L13

- Paglione, T.A.D., Tomaka, T., & Jackson, J.M. 1995, ApJ, 454, L117
- Piner, B.G., Stone, J.M., & Teuben, P.J. 1995, ApJ, 449, 508
- Prada, F., Gutierrez, C.M., & McKeith, C.D. 1998, ApJ, 495, 765
- Pence, W.D., 1981, ApJ, 247, 473
- Peng, R., Zhou, S., Whiteoak, J. B., Lo, K., Y., & Sutton, E. C. 1996, ApJ, 470, 821
- Puche, D., Carignan, C. & van Gorkom, J.H. 1991, AJ, 101, 456
- Sandage, A. & Tammann, G.A. 1975, ApJ, 196, 313
- Shulz, H., & Wegner, G. 1992, A&A, 266, 167
- Scoville, N. Z., Soifer, B. T., Neugebauer, G., Young, J. S., Matthews, K., & Yerka, J. 1985,
289, 129
- Telesco, C. M., & Harper, D. A. 1980, ApJ, 235, 392
- Ulrich, M. 1978, ApJ, 219, 424
- Ulvestad, J. S. & Antonucci, R. R. J. 1997, ApJ, 488, 621
- Watson, A.M., Gallagher, J.S., Hotzman, J.A., Hester, J.J., Mould, J.R., Ballester, G.E.,
Burrows, C.J. 1996, AJ, 112(2), 534

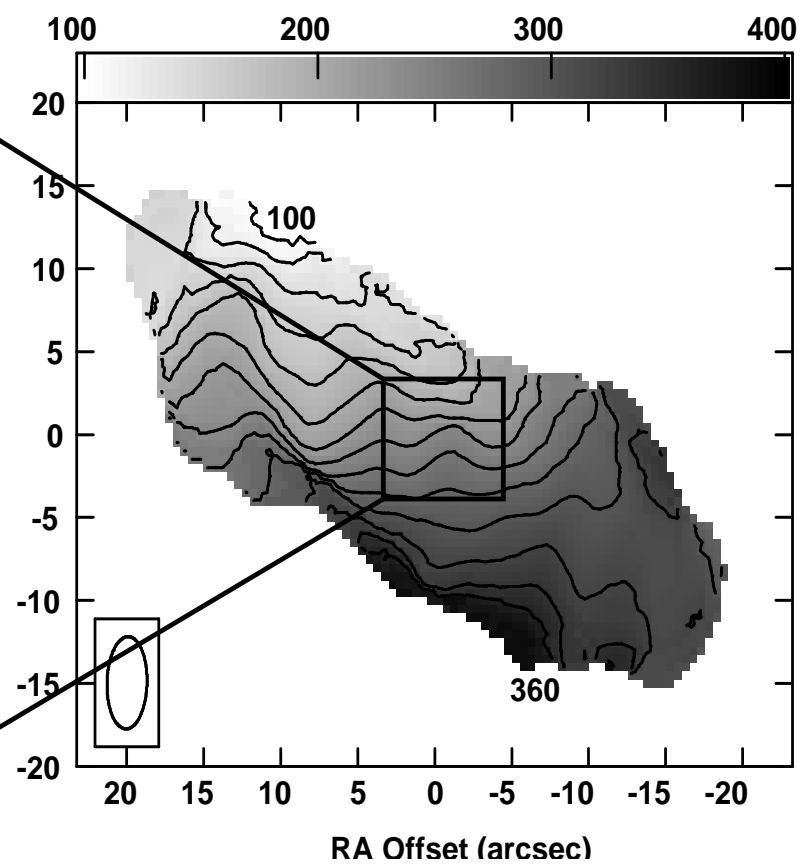
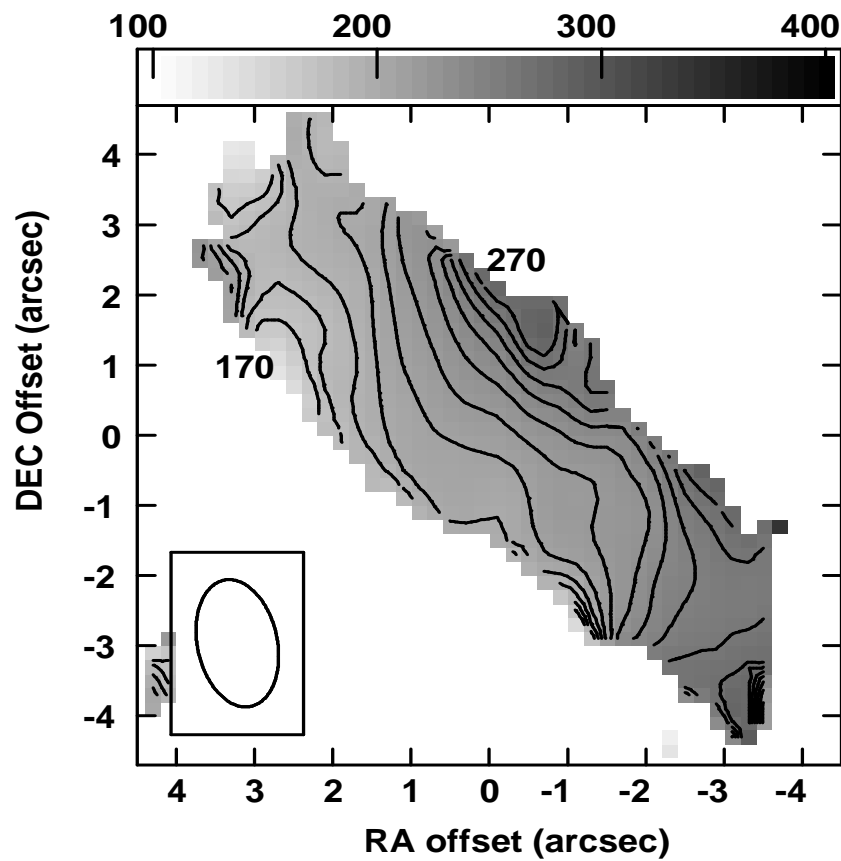
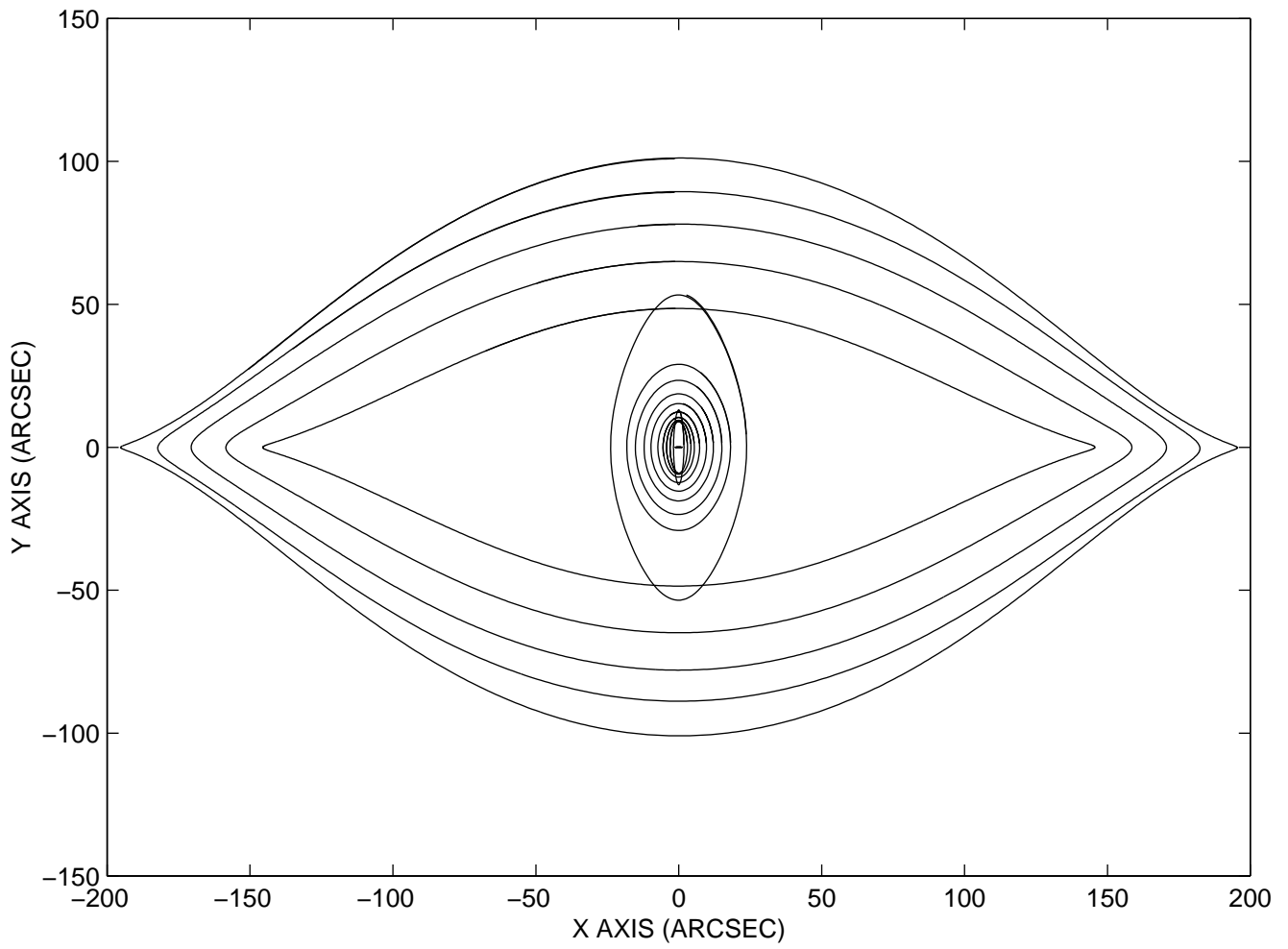
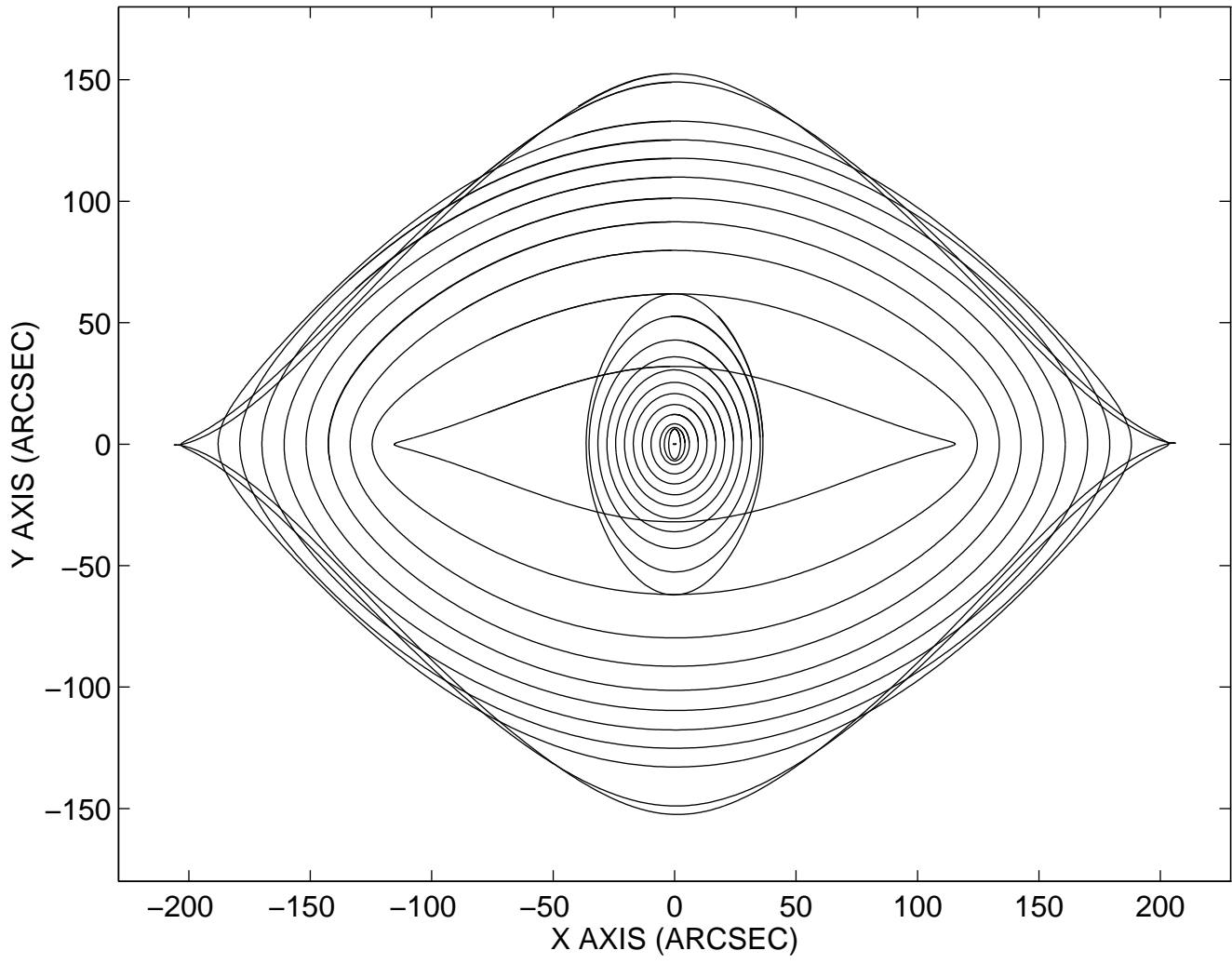


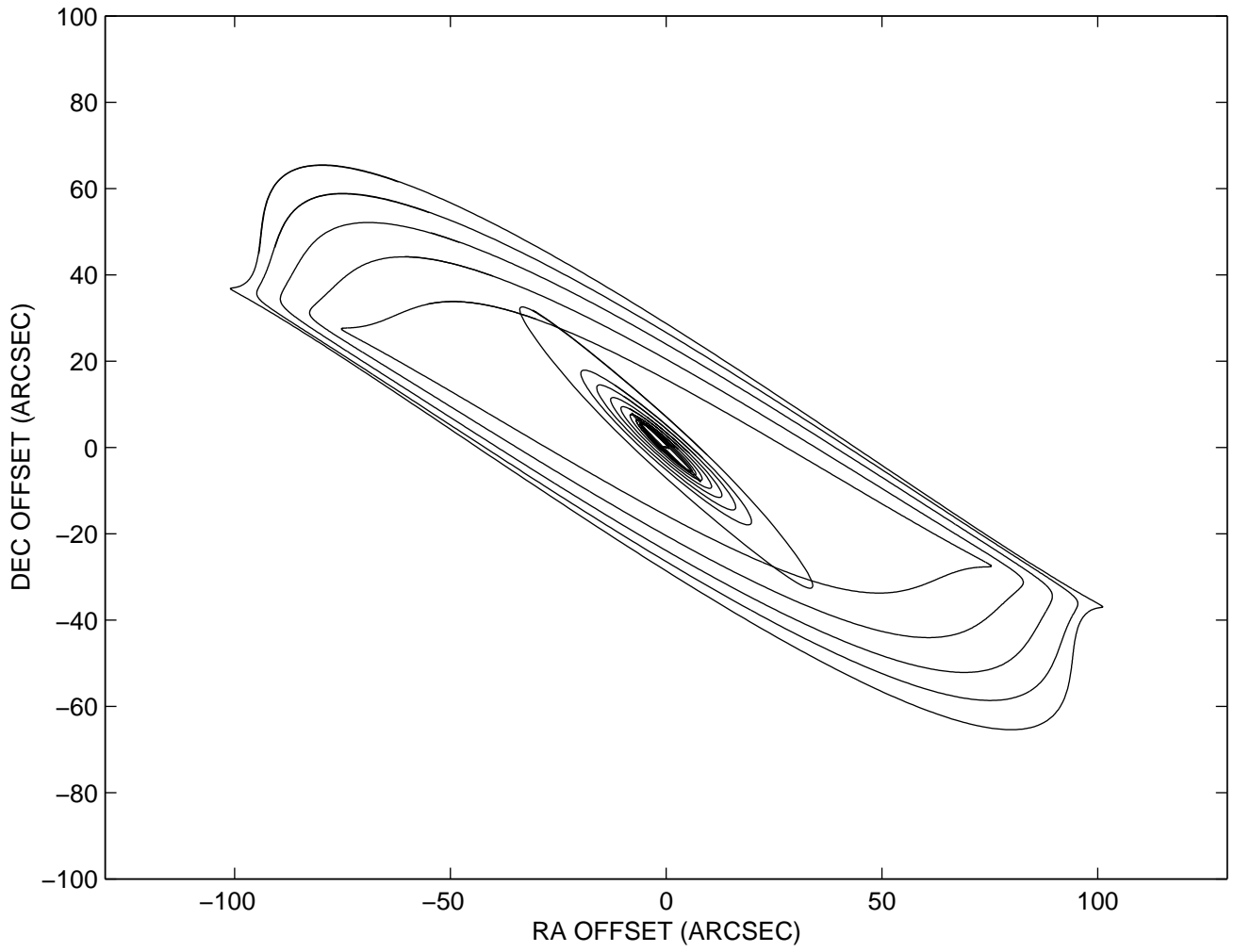
TABLE 1
PARAMETERS OF THE GALAXY NGC 253

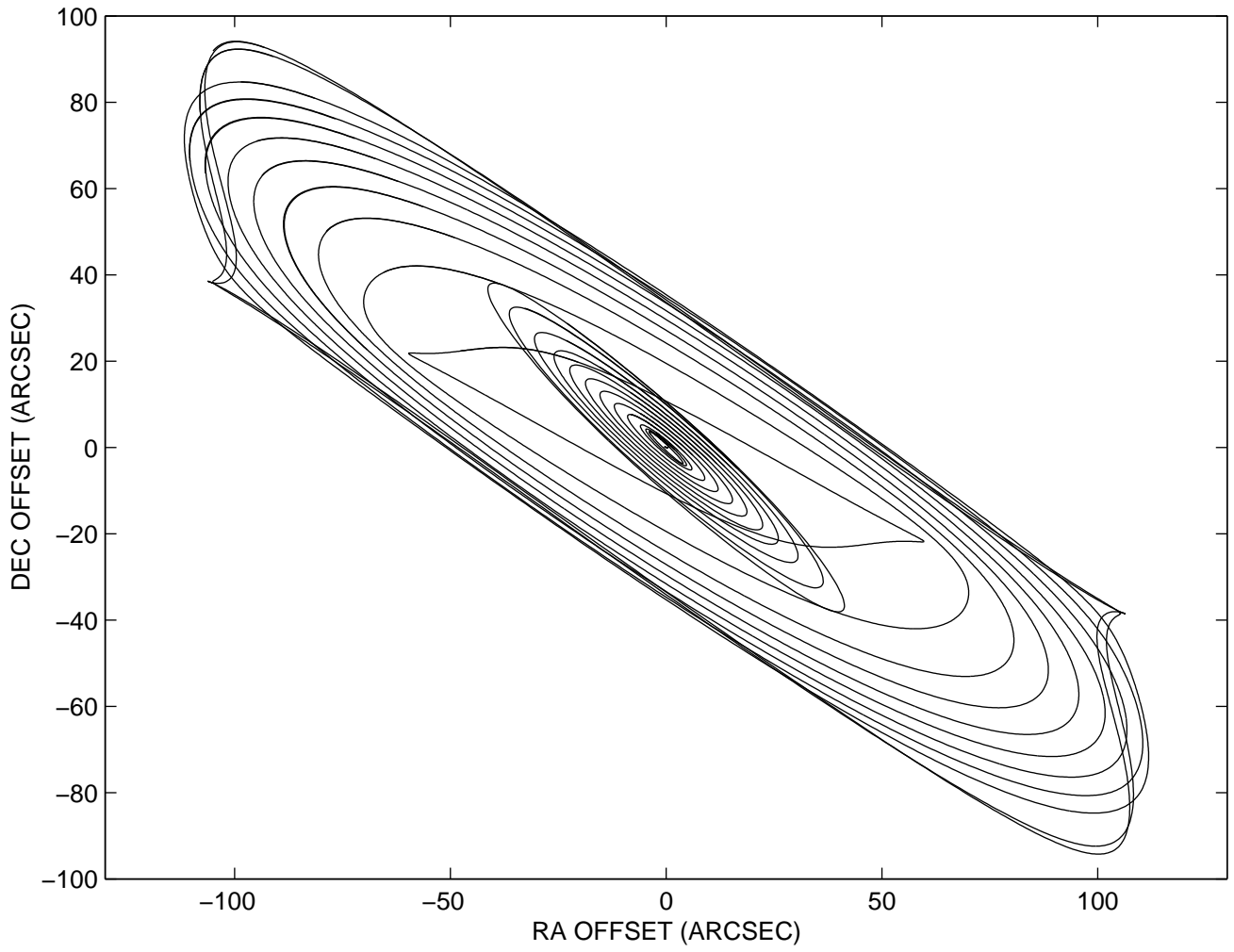
Parameter	Value	Reference
Inclination angle (i)	78.5°	1
PA of galactic disk	52°	2
PA of galactic bar	70°	2
Distance	3.4 Mpc	3
Linear size scale	16.5 pc arcsec ⁻¹	3
Central line velocity (V_{sys})	220 km s ⁻¹	4
Disk rotation speed (V_b)	200 km s ⁻¹	2
Bar angular rotation speed (Ω_b)	48 km s ⁻¹ kpc ⁻¹	2

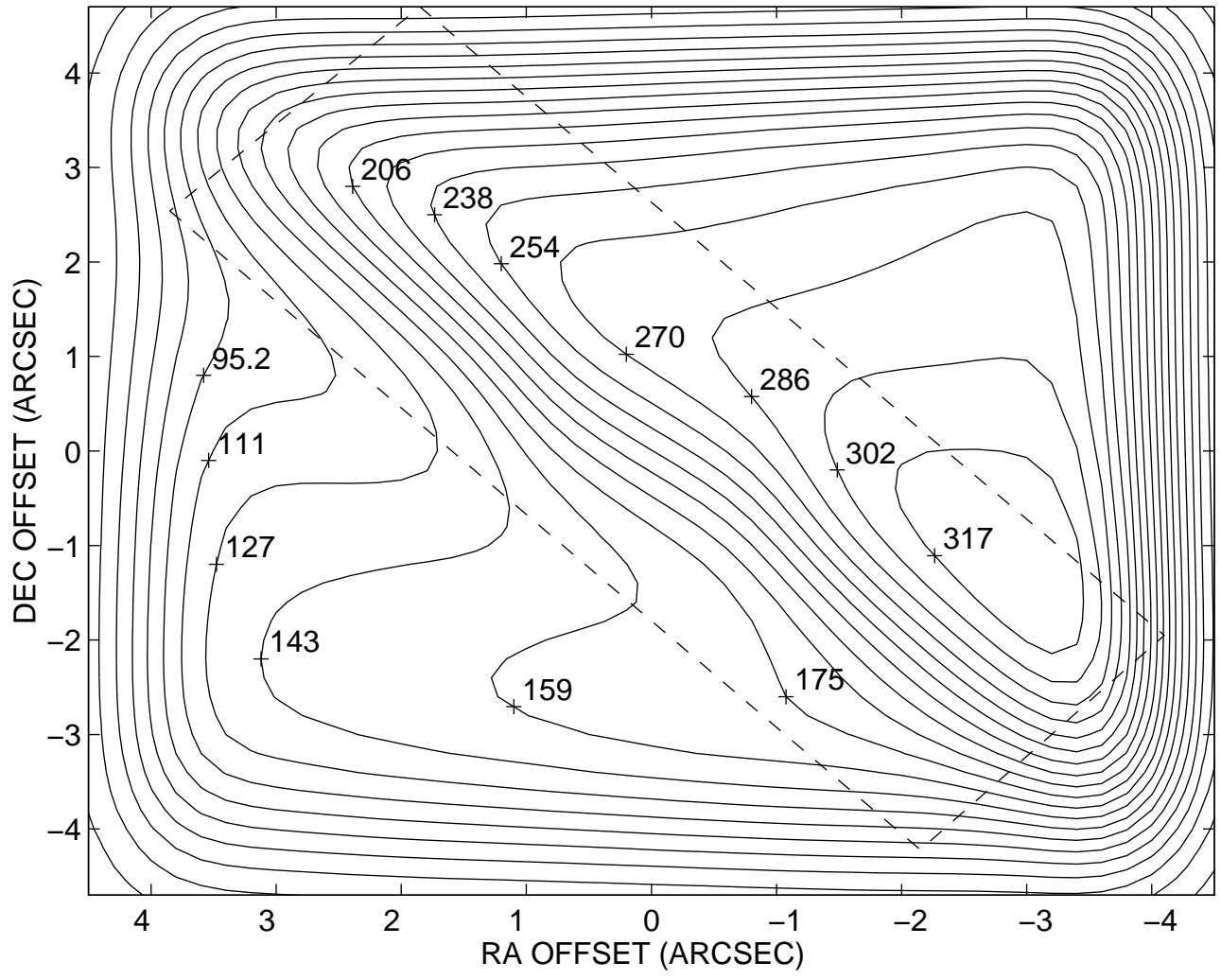
REFERENCES.— (1). Pence, 1981; (2) Arnaboldi et al. 1995; (3) Sandage & Tammann, 1975; (4) Anantharamaiah & Goss, 1996

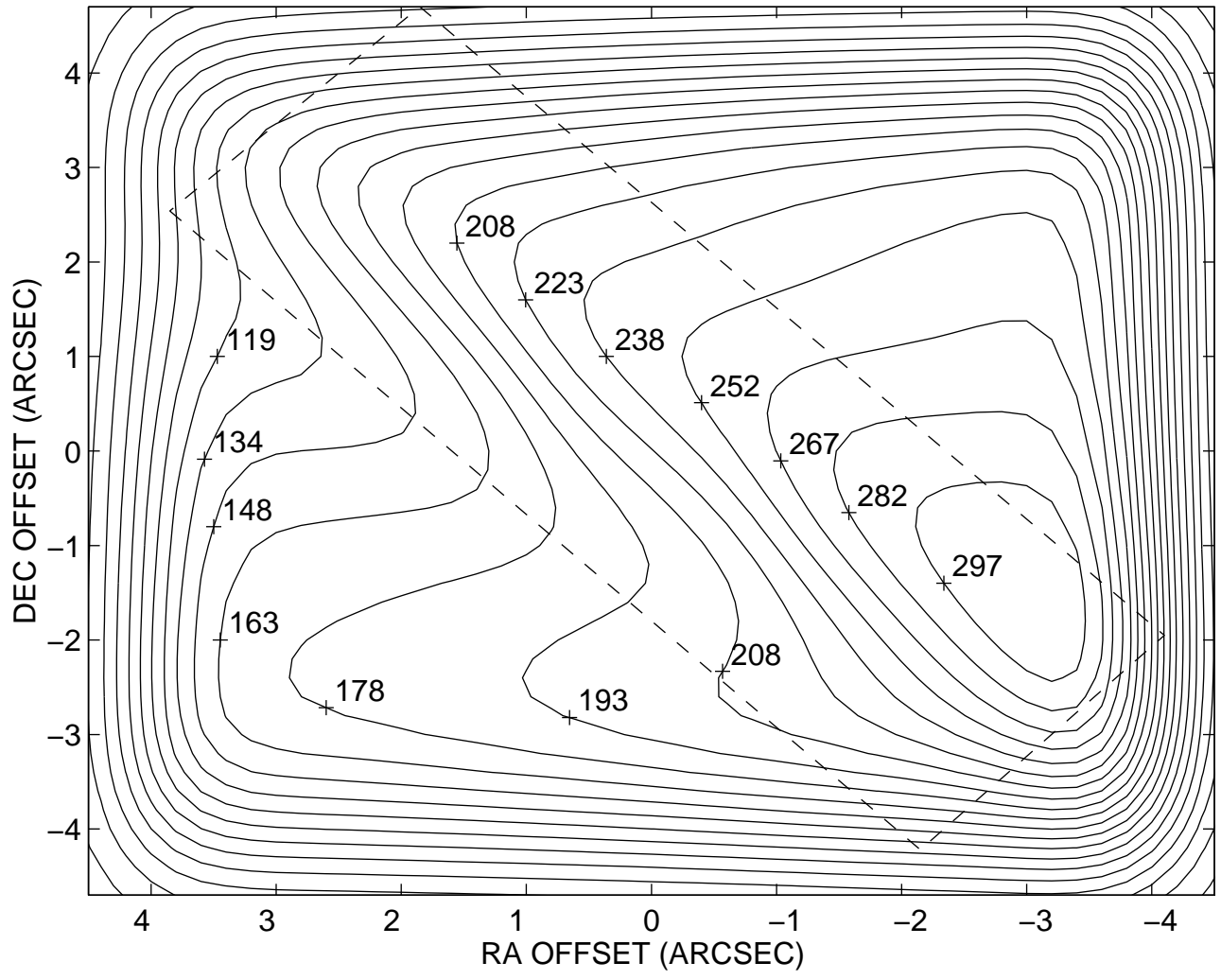


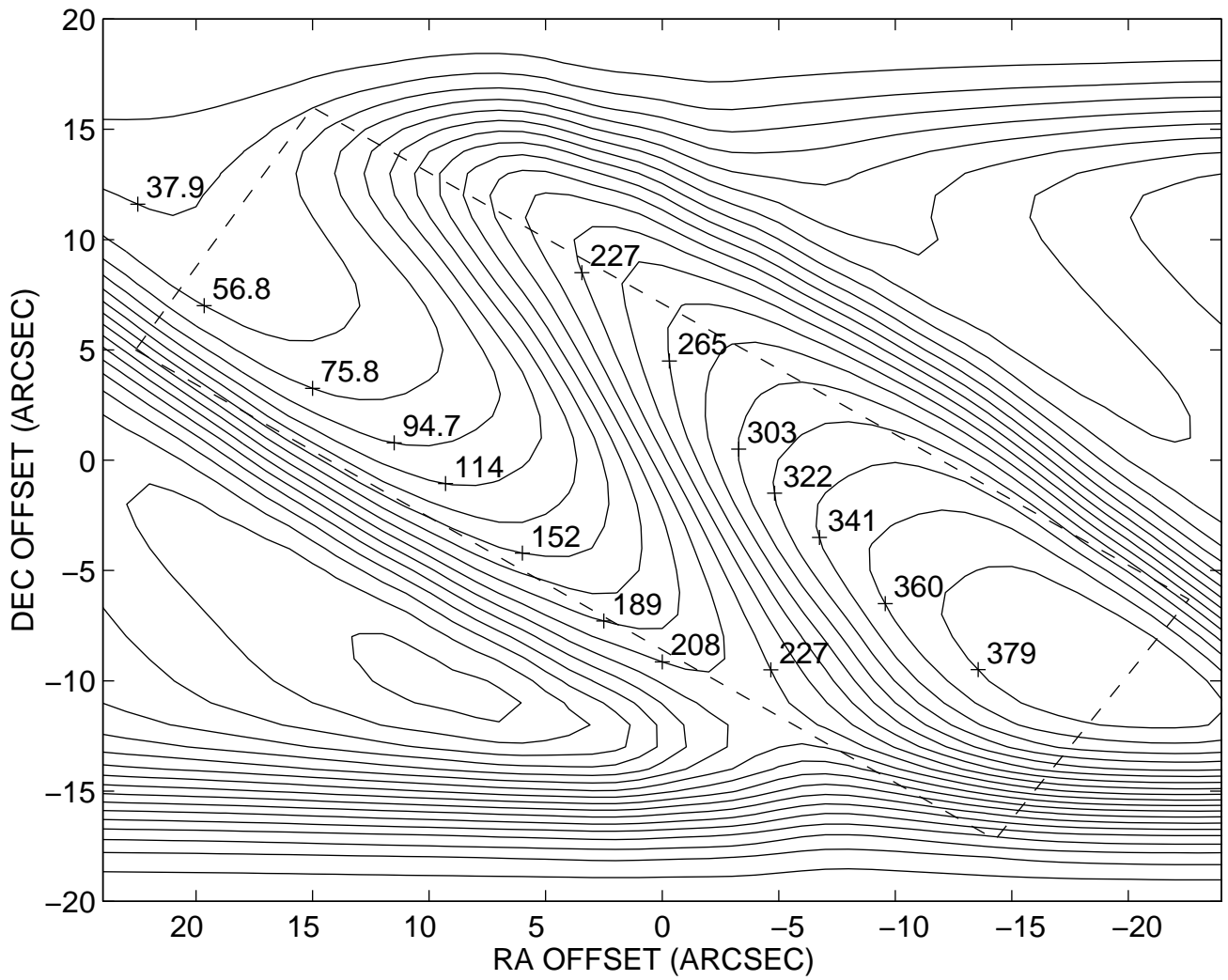


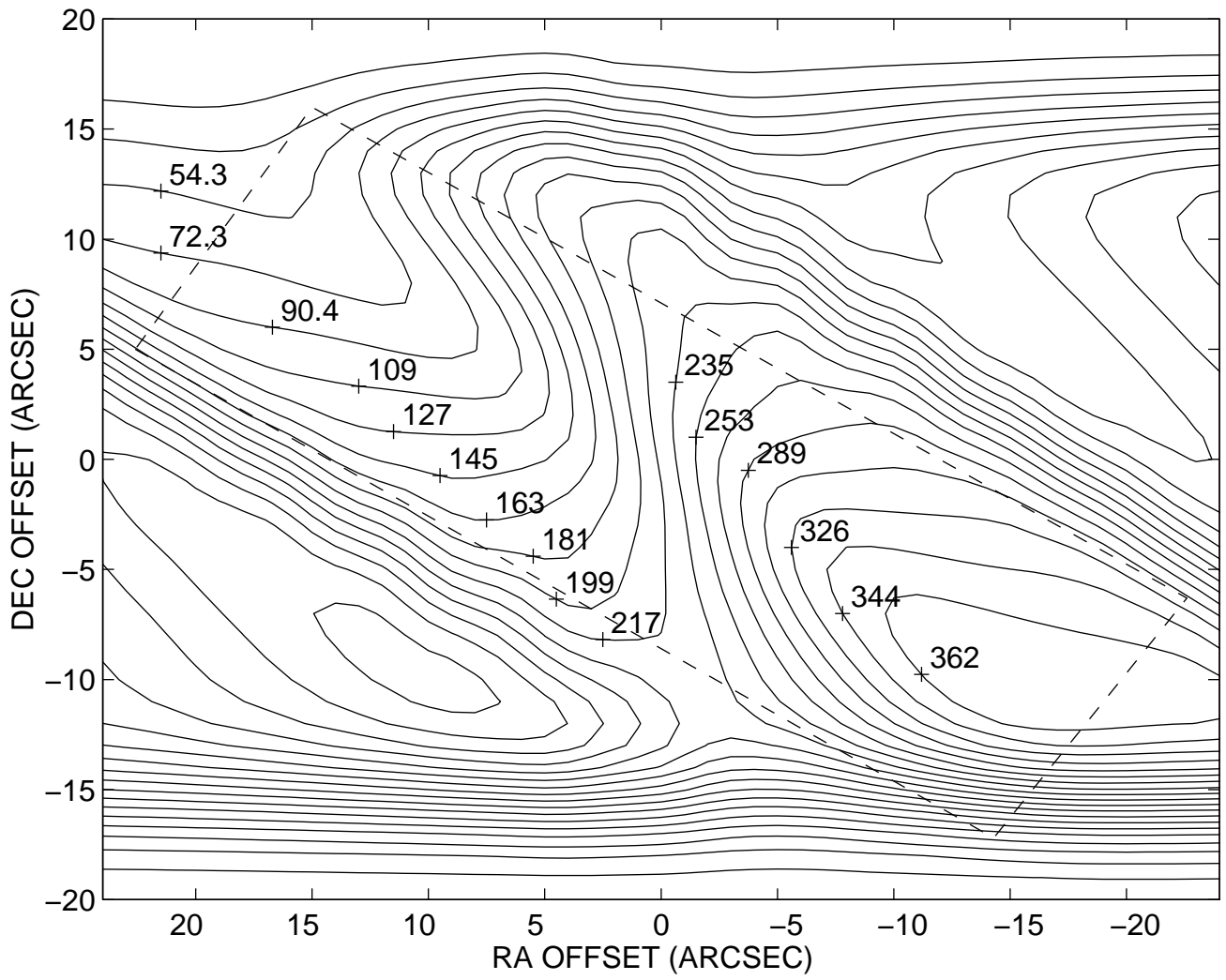


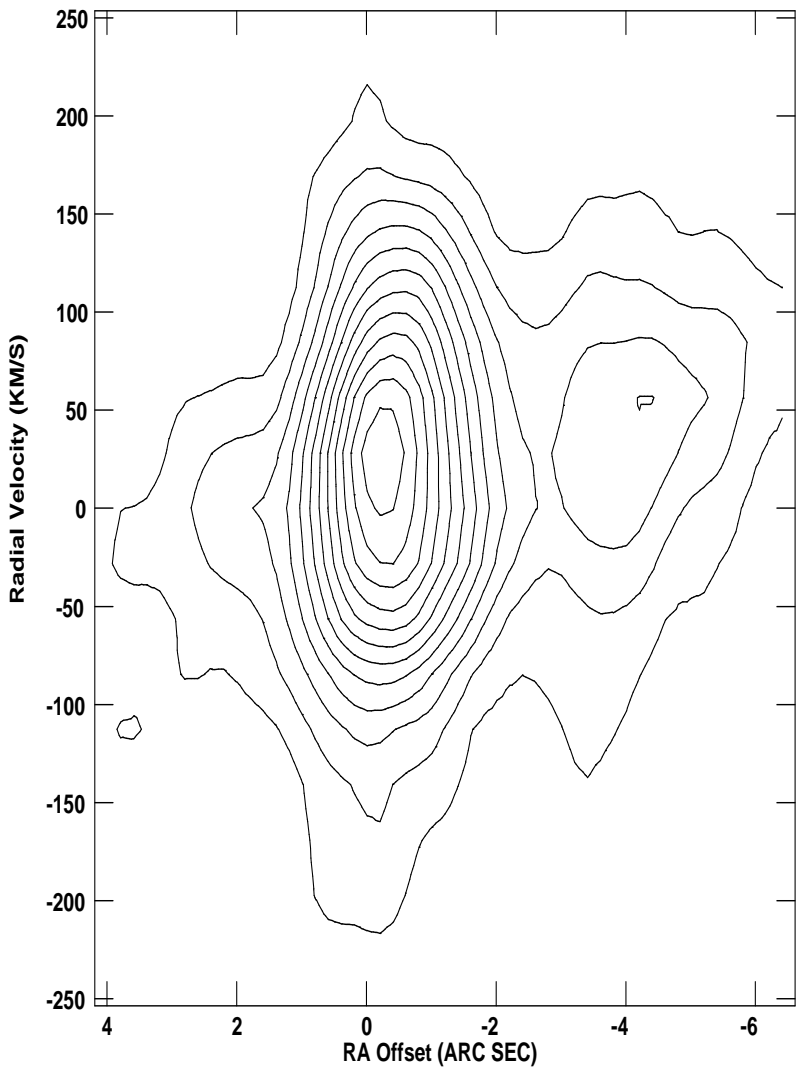


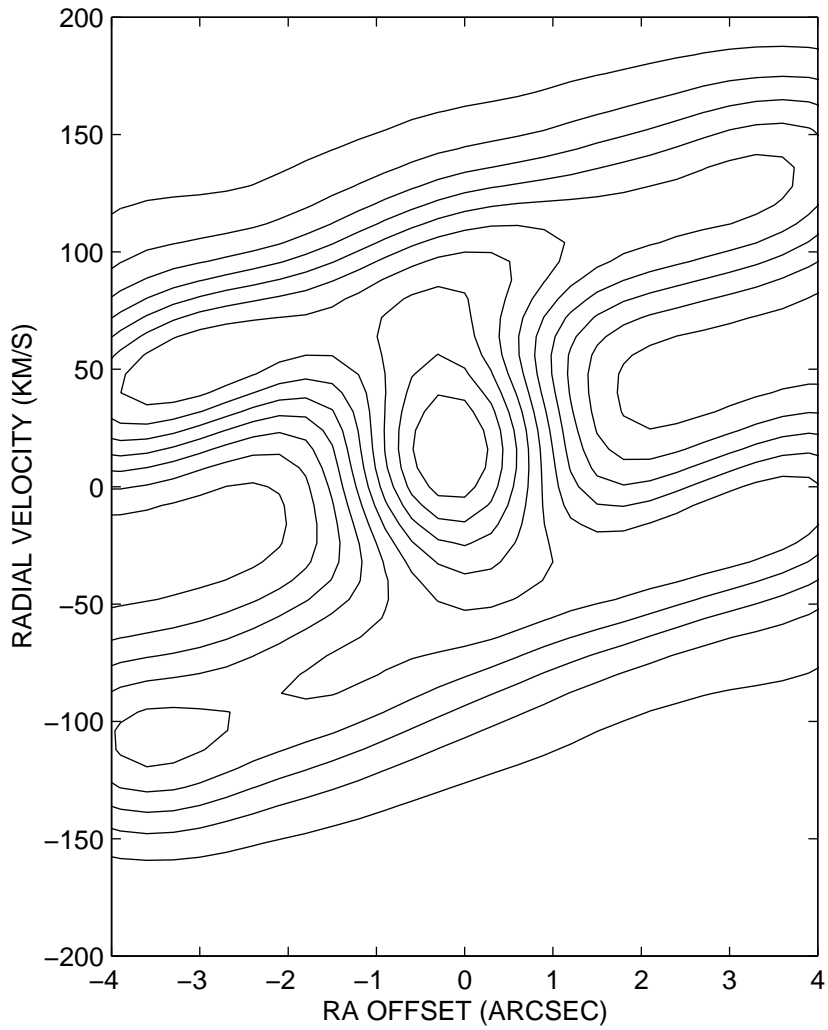












CO Line Brightness (Jy/beam)

